Supplemental document for: A thermodynamically consistent diffuse interface model for the wetting phenomenon of miscible and immiscible ternary fluids

Fei Wang[1,2]†, Haodong Zhang[1,2]‡, Yanchen Wu[1,2], and Britta Nestler[1,2,3]

[1]Institute of Applied Materials-Microstructure Modelling and Simulation, Karlsruhe Institute of Technology, Straße am Forum 7, 76131 Karlsruhe, Germany

[2]Institute of Nanotechnology, Karlsruhe Institute of Technology, Hermann-von-Helmholtz-Platz 1 76344 Eggenstein-Leopoldshafen, Germany

[3]Institute of Digital Materials Science, Karlsruhe University of Applied Sciences, Moltkestraße 30, Karlsruhe 76133, Germany

S.1. Calculation of the stream function based on Huh & Scriven

By defining the stream function

$$u_r = -\frac{1}{r}\frac{\partial \psi}{\partial \varphi},$$
$$u_\varphi = \frac{\partial \psi}{\partial r},$$

we have the bi-harmonic equation for ψ

$$\nabla^2 \nabla \psi_i = 0,\ i = \alpha,\ \delta.$$

The general solution in the polar coordinate for a bounded velocity is expressed as (Huh & Scriven 1971)

$$\psi_i(r,\varphi) = r(a_i \sin\varphi + b_i \cos\varphi + c_i \varphi \sin\varphi + d_i \varphi \cos\varphi),\ i = \alpha,\ \delta.$$

The eight unknowns a_i, b_i, c_i, d_i in the two phases are determined by the following eight boundary conditions (1-8).

-(1,2,3,4) The normal velocities of both phases at the solid-liquid and fluid-fluid interface are zero

$$\frac{\partial \psi_\alpha}{\partial r}|_{\varphi=\theta} = 0;$$
$$\frac{\partial \psi_\alpha}{\partial r}|_{\varphi=\pi} = 0;$$
$$\frac{\partial \psi_\delta}{\partial r}|_{\varphi=\theta} = 0;$$
$$\frac{\partial \psi_\delta}{\partial r}|_{\varphi=0} = 0;$$

† Email address for correspondence: fei.wang@kit.edu
‡ Email address for correspondence: haodong.zhang@kit.edu

-(5) At the fluid-fluid interface, the continuity of the velocity in the tangential direction (no-slip)

$$\frac{\partial \psi_\alpha}{\partial \varphi}|_{\varphi=\theta} = \frac{\partial \psi_\delta}{\partial \varphi}|_{\varphi=\theta};$$

-(6) At the fluid-fluid interface, the balance of the tangential stress reads

$$\eta_\alpha \frac{\partial^2 \psi_\alpha}{\partial \varphi^2}|_{\varphi=\theta} = \eta_\delta \frac{\partial^2 \psi_\delta}{\partial \varphi^2}|_{\varphi=\theta};$$

-(7,8) No-slip of the fluid at the solid surface

$$-U = -\frac{1}{r}\frac{\partial \psi_\alpha}{\partial \varphi}|_{\varphi=\pi};$$
$$U = -\frac{1}{r}\frac{\partial \psi_\delta}{\partial \varphi}|_{\varphi=0}.$$

S.2. Jacqmin's leading order analysis

By considering a contact angle of 90° and a viscosity ratio of 1, the stream line is symmetry with respect to the interface. Here, the fluid-fluid interface is at $\varphi = 0°$ and the solid-liquid interface is at $\varphi = -90°$ differing from the analysis of Huh & Scriven. Because of the symmetry, the general solution of the stream function has four unknowns

$$\psi(r, \varphi) = r(a \sin\varphi + b\cos\varphi + c\varphi \sin\varphi + d\varphi\cos\varphi).$$

By applying the four boundary conditions

- The normal velocity at the substrate is zero

$$\frac{\partial \psi}{\partial r}\big|_{\theta=-\frac{\pi}{2}} = 0 \Rightarrow a = c\frac{\pi}{2}.$$

- The symmetry condition leads to

$$\frac{\partial \psi}{\partial \theta}|_{\theta=0} = 0 \Rightarrow a = -d. \tag{S.1}$$

- The normal velocity at the interface is zero

$$\frac{\partial \psi}{\partial r}|_{\theta=0} = 0 \Rightarrow b = 0.$$

- The tangential velocity of the fluid at the substrate is the same as the substrate (no relative motion)

$$-\frac{1}{r}\frac{\partial \psi}{\partial \theta}|_{\theta=-\frac{\pi}{2}} = -1 \Rightarrow a = \frac{\frac{1}{2}\pi}{1-\frac{1}{4}\pi^2}. \tag{S.2}$$

So that the stream function reads

$$\psi(r, \varphi) = r(a\sin\varphi - a\varphi\cos\varphi - c\varphi\cos\varphi).$$

The Laplace equation for the chemical potential in the polar coordinate (2D) reads

$$\frac{\partial^2 \mu}{\partial r^2} + \frac{1}{r}\frac{\partial \mu}{\partial r} + \frac{1}{r^2}\frac{\partial^2 \mu}{\partial \varphi^2} = 0. \tag{S.3}$$

For the leading order solution (planar interface), we have two constraints for the r-related terms: (i) $\mathcal{O}(\frac{1}{r^2})$, (ii) as $r \to \infty$, we have the chemical potential at equilibrium, namely

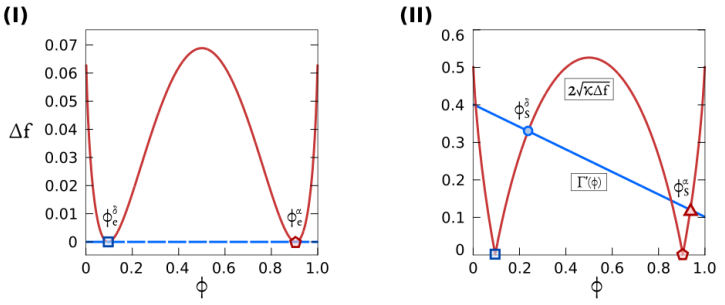

FIGURE S.1. Binary wetting model: (I) The excess free energy density Δf across the interface as a function of ϕ, scaled by f^* (see Tab.S.I). (II) The determination of the surface composition via the intersection of the two curves $\sqrt{2\kappa\Delta f}$ and $\Gamma'(\phi)$, both curves are scaled by the factor of $\sigma*$ (see Tab.S.I). The parameters for the plot is $T = 1$, $\chi = 2.5$, $\kappa = 1$ $a_1 = 0.4$, and $a_2 = -0.3$.

$\mu = 0$. Due to these two constraints, the general solution is proposed as

$$\mu(r, \varphi) = C_1(\varphi)\frac{\ln r}{r} + C_2(\varphi)\frac{1}{r}. \tag{S.4}$$

Substituting Eq. (S.4) into Eq. (S.3), we obtain two ordinary differential equations for the unknowns $C_1(\varphi)$ and $C_2(\varphi)$

$$C_1'' + C_1 = 0, \tag{S.5}$$
$$C_2'' + C_2 - 2C_1 = 0. \tag{S.6}$$

In the case of $\theta = 90°$, the μ profile is symmetry with respect to the interface $\varphi = 0°$. The general solution reads

$$C_1 = A\sin\varphi + B\cos\varphi, \tag{S.7}$$
$$C_2 = -A\varphi\cos\varphi + C\cos\varphi + D\sin\varphi. \tag{S.8}$$

The condition $\frac{\partial\mu}{\partial x} = 0$ at $\varphi = -\pi/2$ results in

$$B = 0,\ C = -\frac{\pi}{2}A. \tag{S.9}$$

The condition $\frac{\partial\mu}{\partial y} = 0$ and $\frac{1}{2}\frac{\partial\mu}{\partial x} = \frac{\partial^3\psi}{\partial y^3}$ at $\varphi = 0°$ couples the Laplace equation with the bi-harmonic equation, resulting in

$$C = 4a. \tag{S.10}$$

The constant a is given by Eq. (S.2). The general solution of the Laplace and bi-harmonic equations consists of the leading order analysis plus the near-field solution. As demonstrated in Jacqmin (2000), the near-field solution only has *numerical* solutions, which are nothing but the present numerical strategy.

S.3. Surface composition for the binary phase-field model

Fig. S.1 shows the determination of the surface composition for the binary phase-field model based on Cahn's theory (Cahn 1977). The intersection of the two curves $2\sqrt{\kappa\Delta f}$ and $\Gamma'(\phi)$ gives rise to the surface composition. The surface compositions ϕ_S^δ and ϕ_S^α correspond to the equilibrium values at the substrate contacting the δ and α phases, respectively.

S.4. Young's law and natural boundary condition

For the binary a-b system, the bulk equilibrium condition $\delta\mathcal{F}/\delta\phi = \mu^{\mathrm{e}}$ leads to

$$\frac{\partial f}{\partial \phi} - 2\kappa\nabla^2\phi = \mu^{\mathrm{e}}. \tag{S.1}$$

Both sides of Eq. (S.1) multiplying by $\nabla\phi$ and integrating once with the condition that the composition gradient vanishes at the boundary give rise to

$$f(\phi) - f(\phi_e^a) - \mu^e(\phi - \phi_e^a) = \kappa(\nabla\phi)^2.$$

By using this equilibrium condition, the interfacial tension is calculated as

$$\gamma_{ab} = 2\kappa\int_{-\infty}^{\infty}(\nabla\phi)^2 dX. \tag{S.2}$$

For a flat substrate with the normal vector $\boldsymbol{n} = [0, 1, 0]$, the surface equilibrium condition is depicted by the following equation

$$2\kappa\, d\phi/dy = d\,\Gamma/d\phi.$$

Multiplying by $d\phi/dm$ where m denotes the normal direction of the droplet-matrix interface at the triple junction, and integrating from $-\infty$ to ∞ yield

$$\int_{-\infty}^{\infty} 2\kappa\left(\frac{d\phi}{dy}\frac{d\phi}{dm}\right)dm = \int_{-\infty}^{\infty} 2\kappa\left(\frac{d\phi}{dm}\right)^2\cos\theta dm = \int_{-\infty}^{\infty}\frac{d\,\Gamma}{d\phi}\frac{d\phi}{dm}dm = \int_{\phi_S^\alpha}^{\phi_S^\delta}\frac{d\,\Gamma}{d\phi}d\phi,$$

where the intersection angle between y and m is the Young's angle θ. If the surface compositions are identical to the equilibrium values of the bulk region, we have $\phi_e^a = \phi_S^a$. Hence, with the equation Eq. (S.2) and the condition that $\Gamma(\phi_e^a) = \gamma_{aS}$, we obtain

$$\gamma_{\alpha\delta}\cos\theta = \gamma_{\delta S} - \gamma_{\alpha S}.$$

It is highly noteworthy that if the surface composition is not equivalent to the bulk composition, the integration should be calculated as

$$\int_{-\infty}^{\infty} 2\kappa\frac{d\phi}{dy}\frac{d\phi}{dm}dm = \int_{\phi_S^\alpha}^{\phi_e^\alpha} 2\kappa\frac{d\phi}{dy}d\phi + \int_{\phi_e^\alpha}^{\phi_e^\delta} 2\kappa\frac{d\phi}{dy}\frac{d\phi}{dm}dm + \int_{\phi_e^\delta}^{\phi_S^\delta} 2\kappa\frac{d\phi}{dy}d\phi.$$

In the end, we obtain the modified Young's equation

$$\gamma_{\alpha\delta}\cos\theta = \gamma_{\delta S} - \gamma_{\alpha S},$$

with

$$\gamma_{\alpha S} = \Gamma(\phi_S^\alpha) + \int_{\phi_S^\alpha}^{\phi_e^\alpha} 2\kappa\frac{d\phi}{dy}d\phi;$$

$$\gamma_{\delta S} = \Gamma(\phi_S^\delta) + \int_{\phi_S^\delta}^{\phi_e^\delta} 2\kappa\frac{d\phi}{dy}d\phi.$$

The derivation for the ternary system is nothing but straightforward.

S.5. Surface equilibrium derivation

At the substrate, the free energy functional is expressed as

$$\mathcal{F} = \int_\Omega \left[\kappa_1(\nabla\phi_1)^2 + \kappa_2(\nabla\phi_2)^2 + \kappa_3(\nabla\phi_3)^2\right] d\Omega + \int_S \Gamma(\phi_1, \phi_2, \phi_3)\, dS.$$

The equilibrium condition $\delta\mathcal{F}/\delta\phi_i = 0$ leads to

$$\int_\Omega -2\kappa_i \nabla^2\phi_i d\Omega + \int_S (\partial\Gamma/\partial\phi_i)\, dS = 0.$$

By using the Gaussian theorem transforming the volume integral into surface integral, we have

$$\int_S -2\kappa_i \nabla\phi_i \cdot \boldsymbol{n}\, dS + \int_S (\partial\Gamma/\partial\phi_i)\, dS = 0.$$

Therefore, the following boundary condition is achieved

$$2\kappa_i \nabla\phi_i \cdot \boldsymbol{n} - \partial\Gamma/\partial\phi_i = 0.$$

S.6. Capillary force and Young-Laplace equation

The increase rate of the kinetic energy for the convection with velocity $\boldsymbol{u}$ due to the capillary force $\boldsymbol{f}_s$ is expressed as

$$\frac{dE_K}{dt} = \int_\Omega \boldsymbol{f}_s \cdot \boldsymbol{u}\, d\Omega.$$

The decrease rate of the free energy is given by

$$\frac{dE_f}{dt} = \int_\Omega \sum_{j=1}^{K-1} \left(\frac{\delta F}{\delta\phi_j} - \frac{\delta F}{\delta\phi_K} \right) \frac{\partial\phi_i}{\partial t} d\Omega,$$

which can be rewritten as by using the convection equation

$$\frac{dE_f}{dt} = -\int_\Omega \sum_{j=1}^{K-1} (\mu_j - \mu_K) \nabla\cdot(\boldsymbol{u}\phi_j)\, d\Omega.$$

By using the Leibniz integration, we obtain

$$\frac{dE_f}{dt} = -\sum_{j=1}^{K-1} (\mu_j - \mu_K)(\mathbf{u}\phi_j)\Big|_{\partial\Omega} + \int_\Omega \sum_{j=1}^{K-1} \phi_j \nabla(\mu_j - \mu_K)\cdot\mathbf{u}\, d\Omega = \int_\Omega \sum_{j=1}^{K-1} \phi_j \nabla(\mu_j - \mu_K)\cdot\mathbf{u}\, d\Omega.$$

With the condition that $dE_f/dt + dE_K/dt = 0$, we obtain the capillary force

$$\boldsymbol{f}_s = -\sum_{j=1}^{K-1} \phi_j \nabla(\mu_j - \mu_K).$$

Considering a droplet with a radius R inside a domain, the equilibrium equation in a polar coordinate reads

$$\mu_i^e = \frac{\partial f}{\partial\phi_i} - 2\kappa_i \Big(\frac{\partial^2\phi_i}{\partial r^2} + \frac{1}{r}\frac{\partial\phi_i}{\partial r} \Big), \quad i = 1, 2, 3.$$

Multiplying by $\partial\phi_i/\partial r$, integrating from 0 (droplet center) to ∞, and summing the three equations yield

$$\Big(f - \sum_{j=1}^{K} \mu_j^e \phi_j^e \Big)\Big|_0 - \Big(f - \sum_{j=1}^{K} \mu_j^e \phi_j^e \Big)\Big|_\infty = \int_0^\infty \frac{2\kappa}{r} \sum_{j=1}^{K} \left(\frac{\partial\phi_j}{\partial r} \right)^2 dr.$$

The right hand side may be approximated by $\gamma_{\alpha\delta}/R$. With the definition of the thermodynamic pressure, $P = f - \sum_{j=1}^{K} \mu_j^e \phi_j^e$, the Young Laplace pressure, $\Delta P = \gamma_{\alpha\delta}/R$ is replicated.

S.7. Energy law

Multiplying both sides of Eq. (6.6) in the main text with $\mathbf{u}$ and integrating over the domain yield the time evolution of the kinetic energy as

$$\frac{d\mathcal{E}}{dt} = \int_\Omega \frac{d}{dt}\Big(\frac{1}{2}\rho\mathbf{u}^2\Big)d\Omega = \int_\Omega \nabla\cdot\Big[\eta\big(\nabla\mathbf{u}+\nabla\mathbf{u}^T\big)\Big]\cdot\mathbf{u}\,d\Omega + \int_\Omega -\nabla p\cdot\mathbf{u}d\Omega + \int_\Omega \mathbf{f}_s\cdot\mathbf{u}\,d\Omega.$$

With the constraint of $\nabla\cdot\mathbf{u}=0$ and no-slip boundary condition, the viscous dissipation is expressed as

$$\int_\Omega \nabla\cdot\Big[\eta\big(\nabla\mathbf{u}+\nabla\mathbf{u}^T\big)\Big]\cdot\mathbf{u}\,d\Omega = -\int_\Omega \eta\nabla\mathbf{u}:\nabla\mathbf{u}\,d\Omega \leqslant 0.$$

By writing the pressure as $-p = -p_0 + f - \sum_{j=1}^K \mu_j\phi_j$, we have $\int_\Omega -\nabla p_0\cdot\mathbf{u}=0$ by using the Leibniz integration with no-slip boundary condition and $\nabla\cdot\mathbf{u}=0$. Combining the rest term in the pressure with $\mathbf{f}_s$ results in

$$\int_\Omega \Big[\mathbf{f}_s + \nabla(f-\sum_{j=1}^K \mu_j\phi_j)\Big]\cdot\mathbf{u}\,d\Omega = -\int_\Omega \sum_{j=1}^K \nabla\cdot\big(2\kappa_j\nabla\phi_j\otimes\nabla\phi_j\big)\cdot\mathbf{u}\,d\Omega.$$

This term corresponds to the Kortweg stress and is cancelled with the time evolution in the free energy functional, as demonstrated in the following.

The time derivative of the free energy functional reads

$$\frac{d\mathcal{F}}{dt} = \int_\Omega \frac{d}{dt}\Big[f(\boldsymbol{\phi}) + \sum_{j=1}^K \kappa_j(\nabla\phi_j)^2\Big]d\Omega + \int_S \frac{d\Gamma(\boldsymbol{\phi})}{dt}dS. \tag{S.1}$$

With the following relation for the total time derivative

$$\frac{d\nabla\phi_i}{dt} = \frac{\partial\nabla\phi_i}{\partial t} + \mathbf{u}\cdot\nabla\nabla\phi_i.$$

Eq. (S.1) is further rewritten as

$$\frac{d\mathcal{F}}{dt} = \int_\Omega \sum_{j=1}^K \Big[\frac{\partial f}{\partial\phi_j}\frac{d\phi_j}{dt} + 2\kappa_j\nabla\phi_j\cdot\nabla\partial_t\phi_j + 2\kappa_j\nabla\phi_j\cdot\mathbf{u}\cdot\nabla\nabla\phi_j\Big]d\Omega + \int_S \frac{d\Gamma(\boldsymbol{\phi})}{dt}dS. \tag{S.2}$$

With the Leibniz integration and denoting the outer and inner normal vector of the substrate as $\hat{\mathbf{n}}$ and $\mathbf{n}$, respectively, Eq. (S.2) reads

$$\begin{aligned}
&\int_\Omega \sum_{j=1}^K \Big[\Big(\frac{\partial f}{\partial\phi_j} - \nabla\cdot 2\kappa_j\nabla\phi_j\Big)\frac{d\phi_j}{dt} + (\nabla\cdot 2\kappa_j\nabla\phi_j)\mathbf{u}\cdot\nabla\phi_j + 2\kappa_j\nabla\phi_j\cdot\mathbf{u}\cdot\nabla\nabla\phi_j\Big]d\Omega \\
&+ \int_S \sum_{j=1}^K \big(2\kappa_j\nabla\phi_j\cdot\hat{\mathbf{n}} + \partial\Gamma/\partial\phi_j\big)\frac{\partial\phi_j}{\partial t}dS \\
&= \int_\Omega \sum_{j=1}^K \Big(\mu_j\frac{d\phi_j}{dt} + \mathbf{f}_j\cdot\mathbf{u}\Big)d\Omega + \int_S \sum_{j=1}^K \big(-2\kappa_j\nabla\phi_j\cdot\mathbf{n} + \partial\Gamma/\partial\phi_j\big)\frac{\partial\phi_j}{\partial t}dS,
\end{aligned} \tag{S.3}$$

where the chemical potential μ_j and the Kortweg force $\mathbf{f}_j$ are defined as

$$\mu_j = \partial f/\partial\phi_j - 2\kappa_j\nabla^2\phi_j, \quad \mathbf{f}_j = \nabla\cdot(2\kappa_j\nabla\phi_j\otimes\nabla\phi_j).$$

Here, we have applied the relation $\nabla\cdot(\nabla\phi_j\otimes\nabla\phi_j) = (\nabla\cdot\nabla\phi_j)\nabla\phi_j + \nabla\phi_j\cdot\nabla\nabla\phi_j$ and assumed the no-slip boundary condition on the substrate, namely $\frac{\partial}{\partial t} = \frac{d}{dt}$, on S. By

applying the following evolution equations

$$\begin{aligned} d_t\phi_i &= \nabla\cdot\left(L_i\nabla\mu_i\right) \quad \text{on} \quad \Omega, \\ \tau_i\partial_t\phi_i &= \left(2\kappa_i\nabla\phi_i\cdot\mathbf{n}-\partial\Gamma/\partial\phi_i\right) \quad \text{on} \quad S, \end{aligned}$$

we obtain the energy dissipation law of the system as

$$\begin{aligned} \frac{d\mathcal{F}}{dt}+\frac{d\mathcal{E}}{dt} =& -\int_\Omega\sum_{j=1}^{K}L_j(\nabla\mu_j)^2d\Omega-\int_S\sum_{j=1}^{K}(1/\tau_j)\left(2\kappa_j\nabla\phi_j\cdot\mathbf{n}-\partial\Gamma/\partial\phi_j\right)^2dS \\ &-\int_\Omega\eta\nabla\mathbf{u}:\nabla\mathbf{u}\,d\Omega\leqslant 0, \quad \forall(\boldsymbol{x},t)\in\Omega\cup S\times[0,T_t]. \end{aligned} \tag{S.4}$$

The additional term $\sum_{j=1}^{K}\mathbf{f}_j\cdot\mathbf{u}$ in the time evolution of the free energy cancels out with the Kortweg stress term in the time evolution of the kinetic energy. Here, L_j and τ_j are mobilities in the bulk and on the substrate S, respectively. These mobilities must be no-negative to fulfill the energy dissipation law. Noteworthily, the mobility can be composition dependent. When the mobility matrix $\mathbf{M}=(M_{ij})\in\mathbb{R}^{K\times K}$ is positive semi-definite, it can be readily shown that the energy law stated in Eq. (S.4) is also satisfied.

Parameters	Description	Expression
x^*	Characteristic length	-
σ^*	Characteristic interfacial tension	-
D^*	Characteristic diffusivity	-
t^*	Time	x^{*2}/D^*
α^*	Ratio of free energy density over surface tension	$(R_gT/v_m)/(\sigma^*/x^*)$
η^*	Dynamic viscosity	$\sigma^*\,x^*/D^*$
u^*	Velocity	D^*/x^*
f^*	Free energy density	$\alpha^*(\sigma^*/x^*)$
ρ^*	Density	$\sigma^*\,x^*/D^{*2}$
p^*	Pressure	σ^*/x^*
τ^*	Time relaxation	σ^**x^{*2}/D^*
M^*	Mobility	D^*/f^*
κ^*	Gradient energy coefficient	σ^*x^*

TABLE S.1. Scaling factors for physical parameters.

S.8. Non-dimensionalization and numerical discretization

All the physical parameters are non-dimensionalized by the characteristic length x^*, reference surface tension σ^*, and diffusivity D^*. These three values are chosen according to the specific time and length scales of the particular system as well as the focused physical process. With these three reference values, we have the following scaling factors for all the other physical parameters, as shown in Tab. S.1. Substituting the scaling factors into the Cahn-Hilliard-Navier-Stokes (CHNS) model, we obtain

$$\frac{\partial\phi_i}{\partial(t^*\widetilde{t})}+\Big(u^*\,\widetilde{\boldsymbol{u}}\Big)\cdot\frac{\widetilde{\nabla}\phi_i}{x^*}=\frac{\widetilde{\nabla}}{x^{*2}}\cdot\left[\sum_{j=1}^{K}\frac{D^*}{f^*}\widetilde{M}_{ij}\widetilde{\nabla}\bigg(f^*\frac{\partial\widetilde{f}}{\partial\phi_j}-\frac{2\,\sigma^*\widetilde{\kappa_j}}{x^*}\widetilde{\nabla^2}\phi_j\bigg)\right],$$

$$\rho^*\widetilde{\rho}\,u^*\bigg(\frac{\partial\widetilde{\boldsymbol{u}}}{\partial(t^*\,\widetilde{t}\,)}+\widetilde{\boldsymbol{u}}\cdot\frac{\widetilde{\nabla}(u^*\widetilde{\boldsymbol{u}})}{x^*}\bigg)=\sum_{j=1}^{K-1}\phi_j\frac{\widetilde{\nabla}}{x^*}f^*\Big(\widetilde{\mu}_K-\widetilde{\mu}_j\Big)-\frac{\widetilde{\nabla}(p^*\widetilde{p})}{x^*}+\frac{\widetilde{\nabla}}{x^*}\cdot\Big[\eta^*\widetilde{\eta}\,u^*\frac{\widetilde{\nabla}(\widetilde{\boldsymbol{u}})+\widetilde{\nabla}(\widetilde{\boldsymbol{u}}^T)}{x^*}\Big],$$

$$\frac{\widetilde{\nabla}}{x^*}\cdot(u^*\,\widetilde{\boldsymbol{u}})=0,$$

$$\tau^*\widetilde{\tau}_i\frac{\partial\phi_i}{\partial t^*\widetilde{t}}=2\sigma^*x^*\widetilde{\kappa}_i\bigg(\frac{\widetilde{\nabla}}{x^*}\phi_i\bigg)\cdot\boldsymbol{n}-\sigma^*\frac{\partial\widetilde{\Gamma}}{\partial\phi_i}.$$

After simplification, the non-dimensionalized form of the CHNS equation reads

$$\frac{\partial\phi_i}{\partial\widetilde{t}}+\widetilde{\boldsymbol{u}}\cdot\widetilde{\nabla}\phi_i=\frac{\widetilde{\nabla}}{Pé}\cdot\left[\sum_{j=1}^{K}\widetilde{M}_{ij}\widetilde{\nabla}\bigg(\frac{\partial\widetilde{f}}{\partial\phi_j}-\frac{2\widetilde{\kappa_j}}{\alpha^*}\,\widetilde{\nabla^2}\phi_j\bigg)\right],$$

$$\widetilde{\rho}\bigg(\frac{\partial\widetilde{\boldsymbol{u}}}{\partial\widetilde{t}}+\widetilde{\boldsymbol{u}}\cdot\widetilde{\nabla}\,\widetilde{\boldsymbol{u}}\bigg)=-\frac{1}{We}\sum_{j=1}^{K-1}\phi_j\widetilde{\nabla}\Big(\widetilde{\mu}_j-\widetilde{\mu}_K\Big)-\frac{\widetilde{\nabla}\widetilde{p}}{We}+\frac{1}{Re}\widetilde{\nabla}\cdot\Big[\widetilde{\eta}(\widetilde{\nabla}\,\widetilde{\boldsymbol{u}}+\widetilde{\nabla}\,\widetilde{\boldsymbol{u}}^T)\Big],\quad\text{(S.1)}$$

$$\widetilde{\nabla}\cdot\widetilde{\boldsymbol{u}}=0,$$

$$\widetilde{\tau}_i\frac{\partial\phi_i}{\partial\widetilde{t}}=2\,\widetilde{\kappa}_i\widetilde{\nabla}\phi_i\cdot\boldsymbol{n}-\frac{\partial\widetilde{\Gamma}}{\partial\phi_i},\ i=1,2,3.$$

The dimensionless quantities Re, We, and $Pé$ are calculated as

$$Re=\frac{\rho^*u^*x^*}{\eta^*},\quad We=\frac{\rho^*u^{*2}x^*}{\sigma^*},\quad Pé=\frac{u^*x^*}{D^*}.$$

The domain Ω is discretized into Ω_N: $[x_1, ..., x_{N_x}] \times [y_1, ..., y_{N_y}] \times [z_1, ..., z_{N_z}]$. The parameters $N_x, N_y, N_z \in \mathbb{N}$ are the number of grid cells in the x, y, and z dimensions, respectively. The substrate S is discretized into S_N: $[x_1, ..., x_{N_x}] \times [z_1, ..., z_{N_z}]$. The time interval $[0, T_t]$ is approximated by $[t_1, ..., t_T]$. The space and time steps are defined as $\Delta x = x_{i+1} - x_i$, $\Delta y = y_{j+1} - y_j$, $\Delta z = z_{k+1} - z_k$, and $\Delta t = t_{l+1} - t_l$, respectively. The indexes $l, i, j, k \in \mathbb{N}$. The finite difference method and the explicit Euler scheme are implemented to solve the evolution equations Eqs. (S.1) with the equidistant Cartesian mesh on a staggered grid, as shown in Fig. S.2(I). The blue and red cells with a size of $\Delta x = \Delta y = \Delta z$ are for the time evolution of the composition in the bulk region Ω and on the substrate S, respectively. In the staggered mesh, the scalar variables, such as composition ϕ_i and pressure p, are represented by the solid points for the bulk and hollow dots for the substrate. The vector variables, such as velocity $\boldsymbol{u}$ and gradient of composition $\nabla\phi_i$, in the x (or z) and y directions are depicted by the triangle, square symbols, respectively, which locate on the border of two adjacent cells as defined by the upwind scheme. We adopt Neumann boundary conditions for compositions $\boldsymbol{\phi}$ on the boundary of bulk region $\partial\Omega$, no-flux boundary condition for the chemical potential on $\partial\Omega$ and substrate S, no-slip boundary condition for the velocity on $\partial\Omega$ and S. The time step Δt for the explicit Euler scheme is chosen according to the von Neumann stability analysis as (Wang *et al.* 2012)

$$\Delta t < \zeta \min\left\{ \frac{Re}{3}\Big(\frac{1}{\Delta x^2} + \frac{1}{\Delta y^2} + \frac{1}{\Delta z^2}\Big)^{-1}, \frac{\Delta x}{|\boldsymbol{u}_x|_{\max}}, \frac{\Delta y}{|\boldsymbol{u}_y|_{\max}}, \frac{\Delta z}{|\boldsymbol{u}_z|_{\max}}, \Delta t_{\mathrm{CH}} \right\},$$

$$\Delta t_{\mathrm{CH}} = \frac{1}{\frac{2^d \max D_i}{\min\{\Delta x^2, \Delta y^2, \Delta z^2\}} + \frac{2^d \max M\kappa_i}{\min\{\Delta x^4, \Delta y^4, \Delta z^4\}}},$$

where ζ defines a safety parameter less than unity, d is the dimension ($d = 2, 3$), and $|\boldsymbol{u}_x|_{\max}$ and $|\boldsymbol{u}_y|_{\max}$, and $|\boldsymbol{u}_z|_{\max}$ are the maximal velocity in the x, y, and z directions, respectively. The numerical solutions of the evolution equations Eqs. (S.1) are conducted within the phase-field simulation framework Pace3D (Nestler *et al.* 2005; Wang *et al.* 2012; Zhang *et al.* 2022). Parallelization of the numerical algorithm is achieved with Message Passing Interface (MPI) techniques. The simulations are performed on the parallel computer bwUniCluster of Baden-Wuerttemberg equipped with Intel Xeon Gold CPUs in the environment of Red Hat Enterprise. The 2D simulations take about two hours by using 40 cores. The 3D simulations take about one day by using 160 cores.

S.9. Numerical convergence

In this part, we perform simulations on a regular mesh with a size of $(N_x \times \Delta x) \times (N_y \times \Delta y)$. The Navier-Stokes equation is not considered in this section. The mesh fineness (or resolution) $\Delta x = \Delta y$ is varied to testify the convergence of the numerical simulation for the Cahn-Hilliard equation, while fixing $(N_x \times \Delta x)$. The parameters adopted are $\kappa_1 = \kappa_2 = \kappa_3 = 2$, $\tau_1 = \tau_2 = \tau_3 = 1$, $D_1 = D_2 = D_3 = 1$, $g_{33} = 0.2$ and the rest wall free energy density coefficients are $g_{ij} = 0$. The parameters for the free energy density are chosen as displayed in Fig. 1(I) of the main text. At the beginning, a semicircular droplet with a radius $R = 40$ ($\Delta x = 1$) is placed on top of the substrate. As illustrated in Fig. S.3(I), the equilibrium contact angle θ converges to the theoretical value 63° with the reduction in Δx. Based on this analysis and for the sake of simulation accuracy and speed, we choose the resolution $\Delta x = 1.0$ for all the following simulations. Besides, one example for the time evolution of the contact angle towards the equilibrium value is presented in Fig. S.3(II).

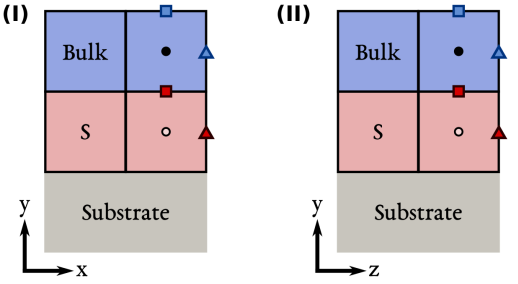

FIGURE S.2. Illustration of the staggered mesh for the numerical discretization: Four neighbouring cells are shown in the figure. The blue and the red regions denote the bulk and the substrate cells, respectively. The size of the cells is $\Delta x = \Delta y = \Delta z$. The solid points represent the scalar variable in the bulk and the hollow points depict the scalar variable on the substrate. The velocity of convection in the x (or z), y dimension is described by the triangle and the square, respectively (red for substrate, blue for bulk). The grey cells are used to represent the bulk of the substrate and not involved for the evolution of the equations. (I) x-y plane; (II) z-y plane.

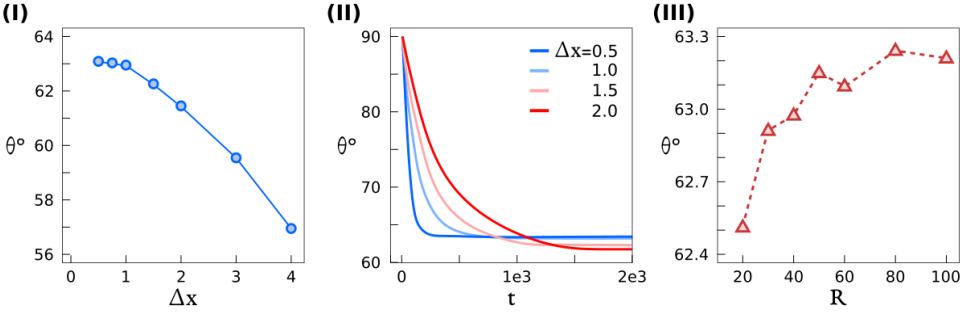

FIGURE S.3. Numerical convergence of the Cahn-Hilliard equation for the contact angle. (I) The convergence of the equilibrium Young's angle θ with reducing mesh fineness Δx for an initial droplet radius $R = 40$. (II) The contact angle θ approaching equilibrium with time for an initial droplet radius $R = 40$ with different mesh fineness Δx, $N_x = 252/\Delta x$, $N_y = 193/\Delta x$. (III) The Young's angle θ with increasing the droplet radius R from simulations. The matrix composition is set to be the equilibrium value according to the binodal line in the phase diagram.

The Young's angle θ for different initial droplet radius R is demonstrated in Fig. S.3(III). Here, the mesh fineness is set as 1.0, while all other simulation parameters are identical to Fig. S.3(I). We observe the deviation of θ for the small droplet, especially when $R = 20$. The reason can be attributed to the curvature effect which changes the equilibrium composition of the droplet. For tiny droplets, its huge curvature results in the enormous composition changes off the equilibrium. Therefore, the composition related surface tension is varied and produces the large deviations of the simulated contact angle compared with larger droplets. As can be noticed in Fig. S.3(III), the contact angle varies with less than 1° for droplets with $R > 40$, which proves the well convergence of our model and of the algorithm measuring the contact angles.

REFERENCES

Cahn, John W 1977 Critical point wetting. *The Journal of Chemical Physics* **66** (8), 3667–3672.

Huh, Chun & Scriven, Laurence E 1971 Hydrodynamic model of steady movement of a solid/liquid/fluid contact line. *Journal of colloid and interface science* **35** (1), 85–101.

Jacqmin, David 2000 Contact-line dynamics of a diffuse fluid interface. *Journal of fluid mechanics* **402**, 57–88.

Nestler, Britta, Garcke, Harald & Stinner, Björn 2005 Multicomponent alloy solidification: phase-field modeling and simulations. *Physical Review E* **71** (4), 041609.

Wang, F, Choudhury, A, Selzer, M, Mukherjee, R & Nestler, B 2012 Effect of solutal marangoni convection on motion, coarsening, and coalescence of droplets in a monotectic system. *Physical Review E* **86** (6), 066318.

Zhang, Haodong, Wang, Fei & Nestler, Britta 2022 Janus droplet formation via thermally induced phase separation: A numerical model with diffusion and convection. *Langmuir* .